Supporting Information

PbS Capped $CsPbI_3$ Nanocrystals for Efficient and Stable Light-Emitting Devices using *p-i-n* Structures

Xiaoyu Zhang, Min Lu, Yu Zhang, Hua Wu, Xinyu Shen, Wei Zhang, Weitao Zheng, Vicki L. Colvin, William W. Yu

Materials: Oleic acid (OA, 90%) and 1-octadecene (ODE, 90%) were purchased from Alfa Aesar. Oleylamine (OLA, 80-90%) was purchased from Aladdin. Thioacetamide (99%) was purchased from J&K. Cs_2CO_3 and PbI_2 were purchased from Sigma-Aldrich.

Synthesis of $CsPbI_3$ NCs: The synthesis procedures were carried out by following a published method (*Nano Lett.,* **2015,** *15*, 3692). Cesium oleate was prepared by adding Cs_2CO_3 (0.814 g), OA (2.5 mL), and ODE (30.0 mL) into a 100 mL three-neck flask, degassed and dried under vacuum for 1 h at 120˚C. Then the mixture was heated to 150˚C under N_2 until a clear solution was obtained. For the preparation of $CsPbI_3$ NCs, 10.0 mL ODE and 0.168 g PbI_2 were loaded into a 50 mL three-neck flask, degassed and dried by applying vacuum for 1 h at 120˚C. Dried OA (1.0 mL) and OLA (1.0 mL) were injected to the flask at this temperature. After the solution became clear, the temperature was raised to 160˚C and 1 mL of cesium oleate solution was quickly injected. Five seconds later, the reaction mixture was cooled down to room temperature by an ice-water bath. The reaction mixture was separated by centrifuging for 10 min at 5000 rpm. Then the precipitate was

redispersed in 3.0 mL of toluene and centrifuged again for 10 min at 10 000 rpm, and redispersed in 2.0 mL of toluene for LED applications.

Synthesis of PbS capped $CsPbI_3$ NCs: To prepare PbS capped $CsPbI_3$ NCs, thioacetamide of different weight was added into 1 mL OLA as sulfur precursor (S-OLA). The weight of thioacetamide added was determined by target products. For example, 0.0028 g thioacetamide was employed to prepare $CsPbI_3$-0.1 NCs. 10.0 mL ODE and 0.168 g PbI_2 were loaded into a 50 mL three-neck flask, degassed and dried by applying vacuum for 1 h at 120˚C. Dried OA (1.0 mL) and S-OLA (1.0 mL) were injected to the flask at this temperature. After the solution became clear, the temperature was raised to 160˚C and 1 mL of cesium oleate solution was quickly injected. Five seconds later, the reaction mixture was cooled down to room temperature by an ice-water bath.

Device fabrication: Patterned ITO-coated glass was carefully cleaned successively using soap, deionized water, ethanol, chloroform, acetone, and isopropanol, and was subjected to UV-ozone treatment for 15 min. A solution of ZnO NCs (50 mg mL^{-1}) was spin-coated onto the ITO glass at 1000 rpm for 1 min and annealed in air at 150˚C for 10 min. Then the substrate was transferred into a N_2 glove-box. A PEI 2-methoxyethanol solution (0.2% mass fraction) was spin-coated onto the ZnO film at a speed of 3000 rpm and annealed at 110˚C for 10 min. The perovskite NC emissive layers (20 mg mL^{-1}) were spin-cast at 1000 rpm for 1 min. TCTA, MoO_3, and Au films were sequentially deposited by thermal evaporation in a vacuum deposition clamber (1×10^{-7} Torr). The thicknesses of electron transporting layer,

emitting layer, hole transporting layer and MoO_3 layer are 45, 60, 40, and 10 nm, respectively.

Characterizations: Absorption and photoluminescence (PL) spectra were measured on a PerkinElmer Lambda 950 spectrometer and a Cary Eclipse spectrofluorimeter, respectively. Transmission electron microscopy (TEM) images were obtained on a FEI Tecnai F20 microscope. Powder XRD data were collected on a Bruker SMART-CCD diffractometer. The absolute PL QYs of the samples were measured on a fluorescence spectrometer (FLS920P, Edinburgh Instruments) equipped with an integrating sphere with its inner face coated with BENFLEC. Time-resolved PL measurements were performed with a time correlated single-photon counting (TCSPC) system of the FLS920P Edinburgh spectrometer. A 379 nm picosecond diode laser (EPL-375, repetition rate 5 MHz, 64.8 ps) was used to excite the samples. Ultraviolet photoelectron spectroscopy (UPS) spectra were collected on a PREVAC system. A Keithley 2612B source meter was used to measure the current−voltage characteristics of the devices. The EL spectra were recorded on a Maya spectrometer (Ocean Optics) coupled to an optical fiber. The LED brightness was determined using a Photo Research Spectra Scan spectrometer PR650.

Fitting and analysis of PL decay curves. The PL decay curves in Figure 1d were bi-exponential fitted. As shown in Table S1, the lifetime in the $CsPbI_3$ NCs reveals the presence of two distinct components with time constants of 2.2 ns and 23.8 ns for the faster and the slower recombination components, respectively. The faster decay component is

owing to the direct radiative recombination of excitons (*Nano Letters*, **2003**, *3*, 1103), and the slower decay component is attributed to the trap-meditative recombination, being described in literatures and suggested by the referee (*Nano Lett.*, **2015**, *15*, 7718). Comparing the lifetime of the PbS capped NCs with the pristine $CsPbI_3$ NCs, the faster decay time constant (τ_1) associated to the direct radiative recombination of excitons is prolonged from 2.2 to 2.3 ns, and the slower decay time constant (τ_2) related to the trap-meditative recombination presents little change. Moreover, the relative ratio of amplitude (f_1) of τ_1 to (f_2) of τ_2 increased obviously. These results indicated that some of the traps have been modified through the capping of the PbS shells, which is consistent with the previous reports.

Table S1. Parameters obtained from the time-resolved photoluminescence study.

	τ_1 (ns)	f_1 (%)	τ_2 (ns)	f_2 (%)	τ_{avg}(ns)
$CsPbI_3$	2.2	24.4	23.8	75.6	16.9
$CsPbI_3$-0.1	2.3	29.1	23.5	70.9	17.4

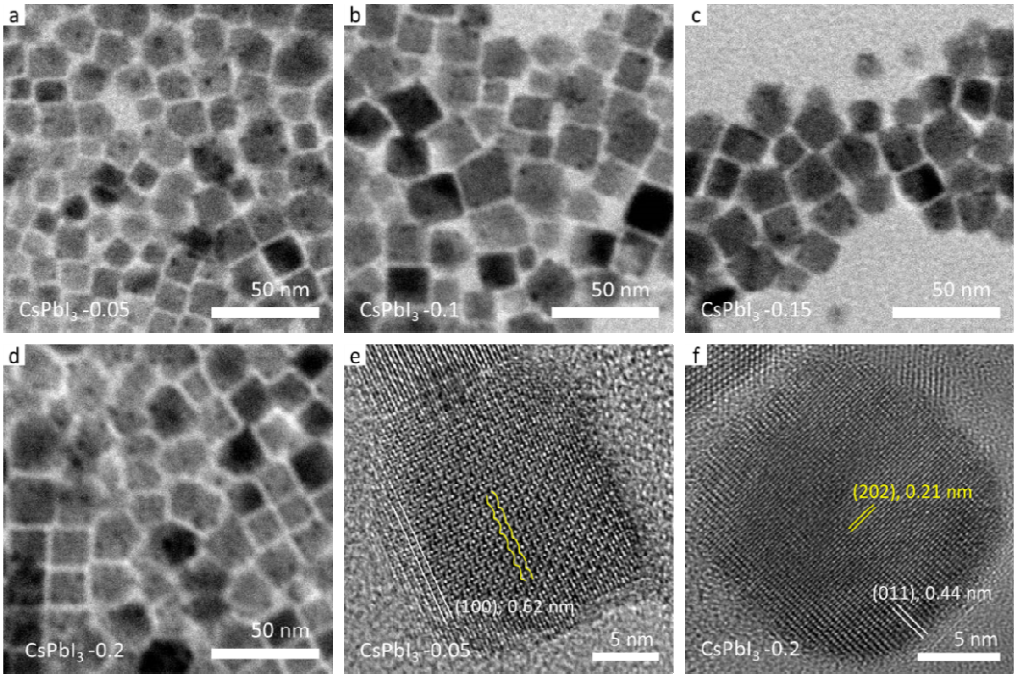

Figure S1. (a), (b), (c), and (d) are TEM images of $CsPbI_3$-0.05, $CsPbI_3$-0.1, $CsPbI_3$-0.15, and $CsPbI_3$-0.2 NCs, respectively. (e) and (f) are HRTEM images of $CsPbI_3$-0.05 and $CsPbI_3$-0.2 NCs, respectively.

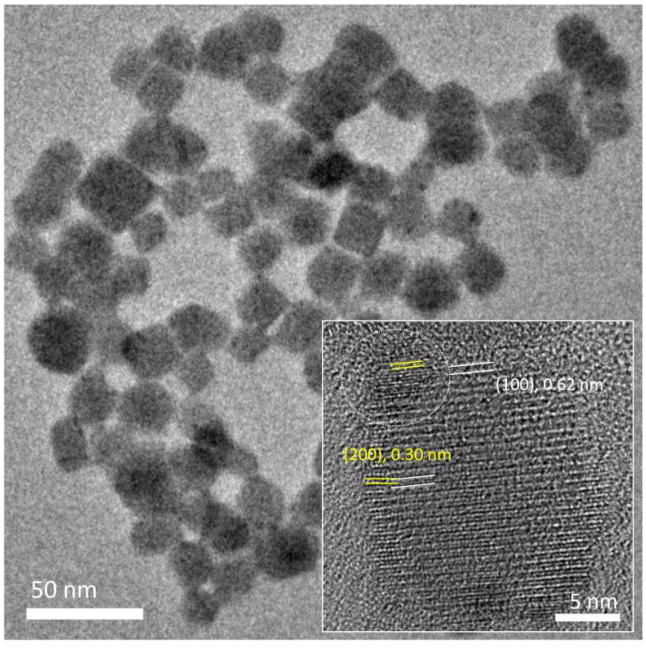

Figure S2. Additional TEM and HRTEM (inset) images of $CsPbI_3$-0.1 NCs.

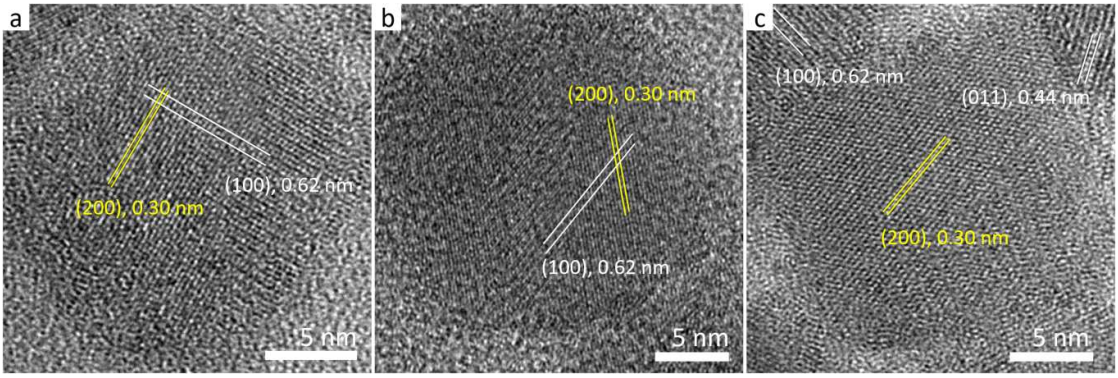

Figure S3. (a), (b), and (c) are additional HRTEM images of PbS capped $CsPbI_3$ NCs.

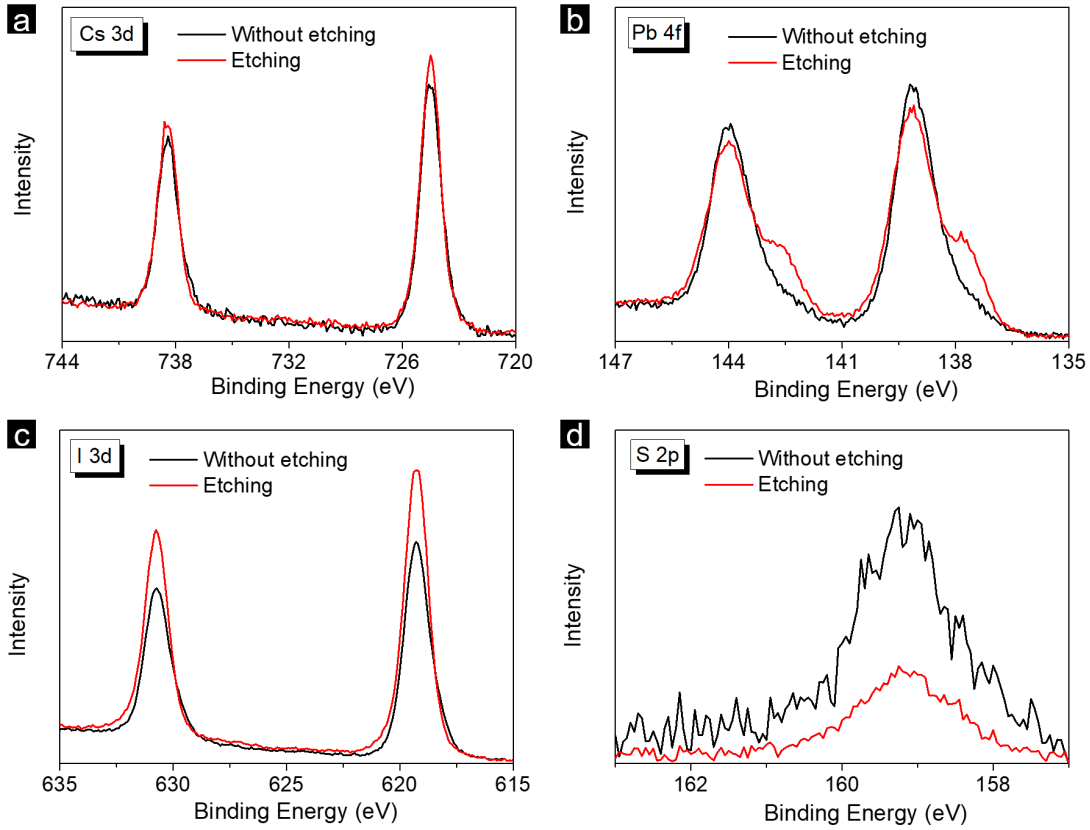

Figure S4. The XPS measurements of PbS capped $CsPbI_3$ NC film at different depth. (a), (b), (c) and (d) are curves for Cs, Pb, I and S, respectively.

In order to clearly observe the element content variation, $CsPbI_3$-0.2 NCs with thick PbS shells were used. As shown in Figure S4, a ~65% decrease in the S contents was observed, while Cs, Pb and I contents exhibited slight increase after removing a top layer by etching, demonstrating the difference between the composition of the core and the composition of the shell. Thus, from the depth XPS results, we conclude that S exists on the $CsPbI_3$ NC surface. There is no peak shift or shape change in the S 2p XPS spectra before and after etching, indicating that the chemical environment around S atoms is the same. The situation is similar for Cs and I atoms. In comparison, the low binding energy peak of Pb^0 in the Pb 4f spectra became obvious after etching.

Figure S5. Photos of $CsPbI_3$-0.1 NC toluene solution under day light and 365 nm excited.

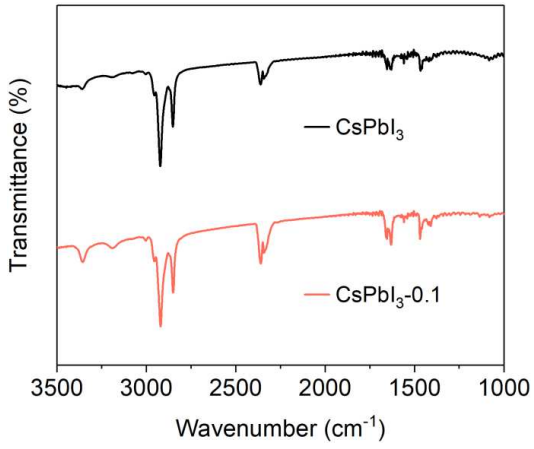

Figure S6. FTIR spectra of $CsPbI_3$ and $CsPbI_3$-0.1 NCs.

Semiconductor property analysis. For pure $CsPbI_3$ NCs, their Fermi level (-3.84 eV) and CBM (-3.78 eV) are close to each other, which clearly identifies their *n*-type behavior. After PbS capping, the Fermi level increases to -4.40 eV while the CBM and VBM values were almost the same, demonstrating the switch from *n*-type behavior to nearly ambipolar.

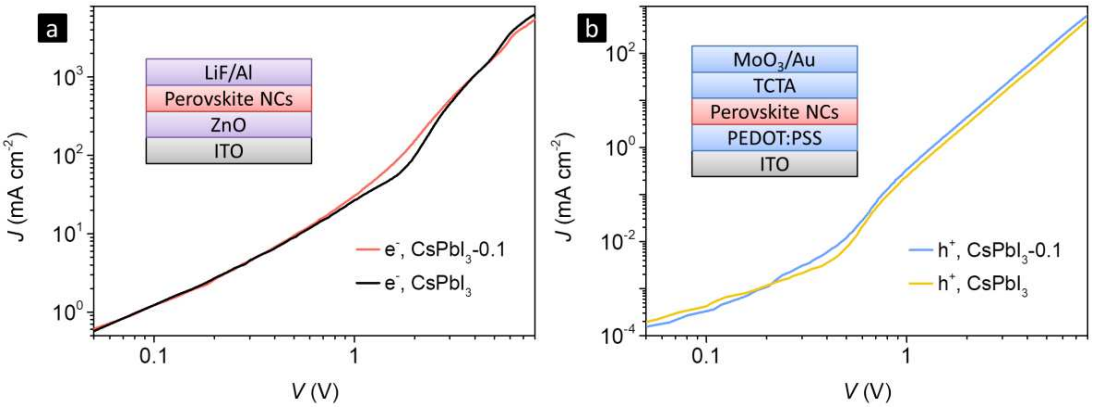

Figure S7. *J-V* curves of (a) "electron-only" and (b) "hole-only" devices.

The "electron-only" and "hole-only" devices were fabricated and compared (Figure S7). The device structures we employed are given as inset. For the electron-only device, the currents keep the same below 5 V even $CsPbI_3$ NCs are *n*-type semiconductors, demonstrating PbS capping have successfully passivated the NC surface. When the voltage is above 5 V, the current of $CsPbI_3$ device is obviously higher than that of PbS capping device, which is benefiting from their *n*-type behavior. For hole-only device, the current of $CsPbI_3$-0.1 device is higher than that of $CsPbI_3$ device, which is as a result of the Fermi level increases and surface passivation.

It is known that the electronic properties of colloidal NCs are critically dependent on their surface chemistry. Through changing the surface ligands, the energy level of PbS NCs can shift by up to 0.9 eV (*ACS Nano*, **2014**, *8*, 5863). By increasing the amount of S, the transport characteristic of PbS NCs would become more *p*-type (*Phys. Rev. Lett.,* **2013**, *110,* 196802).

Metallic Pb atoms can easily develop in perovskite and cause strong exciton quenching, thus pure $CsPbI_3$ NCs are *n*-type with lower PL QY of 65%. After introducing small amount of S, the Pb atoms are passivated while S atoms are introduced to the NC surface (Figure S1e), thus $CsPbI_3$-0.05 NCs are less *n*-type with higher PL QY of 70 %. When the content of sulfur keeps increasing (over 0.05), thick PbS capping are formed (Figure S1f), charges will transfer to PbS at this case, leading to the decrease of PL QY.

On the other hand, the PbS HOMO and LUMO values are highly dependent on the NC size (*ACS Nano,* **2016**, *10*, 3302). Thinner PbS shell offers larger bandgap, which will reduce the energy level difference, weakens the charge transfer driving force, and thus reduces the PL QY decreases.

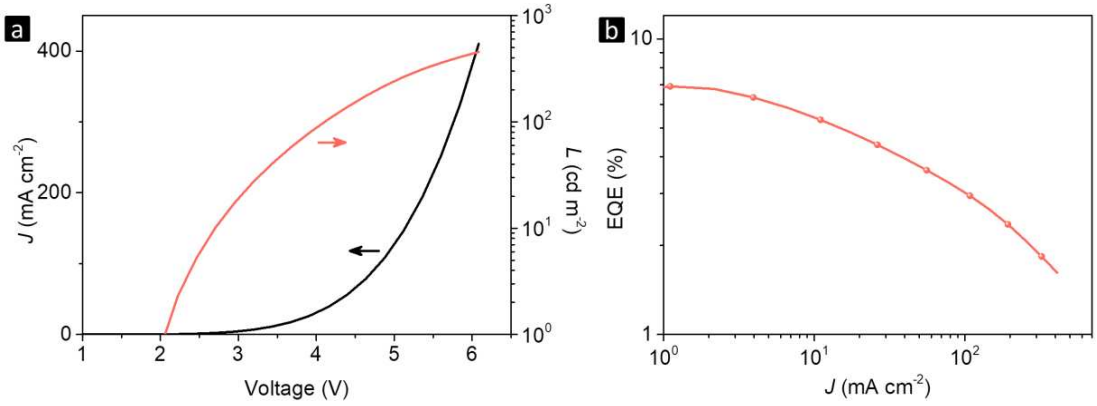

Figure S8. (a) J-V-L and (b) EQE curves of $CsPbI_3$ NC LEDs.

The *J-V-L* curves and EL efficiency of a typical $CsPbI_3$ NC LED are given in Figure S8. The device exhibits a turn-on voltage of 2.1 V, a peak brightness of 455 cd m^{-2}, and a peak EQE of 6.9%. Compared to the device using the nanocrystals without PbS, PbS-capped $CsPbI_3$ nanocrystal-based devices exhibited higher EL efficiency, which reached to 11.8% as shown in Figure 3d.

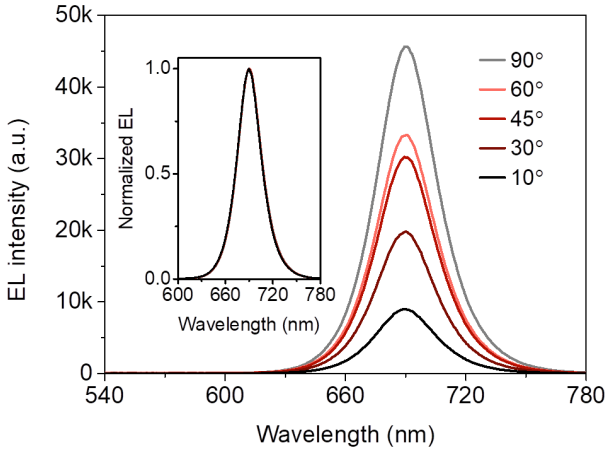

Figure S9. Angle dependent EL spectra.

We measured the angle dependent absolute EL spectra at 4 V that are given in Figure S9, and the normalized EL spectra are given as inset. These curves overlapped each other and no peak shifts have been observed.

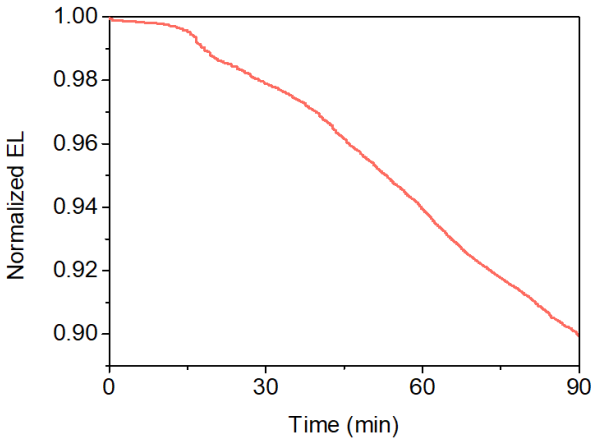

Figure S10. Time related operational stability of $CsPbI_3$-0.1 NC LEDs.

As shown in Figure 4d from the manuscript, the EL intensity of $CsPbI_3$ LEDs decreases to ~50% of their initial value after 600 s, while the EL intensity of a $CsPbI_3$-0.1 LED shows negligible decrease. The stability with longer time was tested, and the normalized EL intensity of a $CsPbI_3$-0.1 LED at a constant voltage of 2.5 V was given in Figure S10. The EL intensity keeps 90% of the initial value after 90 min. This device stability is better or

comparable to some of previously reported results (*Adv. Mater.,* **2017**, *29*, 1606600; *Nature Communications*, **2017**, *8*, 15640), but still not as good as the $CsPbBr_3$ LED with all inorganic charge transporting layers (*Nano Lett.*, **2017**, *13*, 313), which is mainly limited by the device structure.

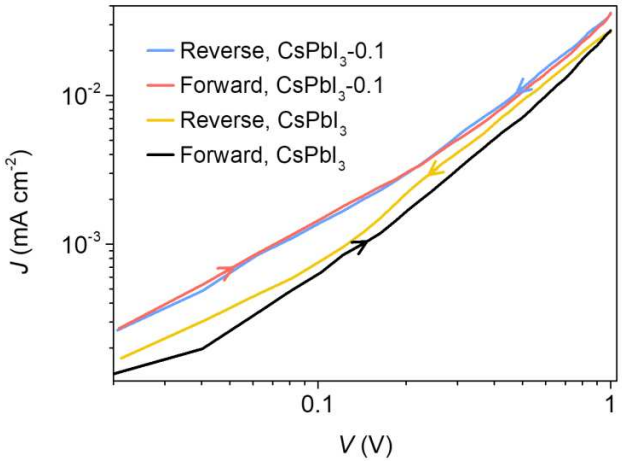

Figure S11. The *J-V* curves of $CsPbI_3$ and $CsPbI_3$-0.1 devices measured under reverse and forward voltage scans.

We find $CsPbI_3$-0.1 device clearly shows smaller hysteresis, demonstrating that PbS capping can help to stabilize ion migration. PbS capping helps to stabilize the NC surface and impede ion migration, thus improved the operation stability of LEDs.